Pergamon

Int. J. Heat Mass Transfer. Vol. 40, No. 11, pp. 2655–2670, 1997

Printed in Great Britain
0017-9310/97 $17.00+0.00

PII: S0017-9310(96)00278-5

Two-fluid modelling of inverted annular film boiling

N. HAMMOUDA
Mechanical Engineering Department, University of Ottawa, Ottawa, Ontario K1N 6N5, Canada

D. C. GROENEVELD
Fuel Channel Thermalhydraulics Branch, AECL, Chalk River, Ontario K0J 1J0, Canada

and

S. C. CHENG†
Mechanical Engineering Department, University of Ottawa, Ottawa, Ontario K1N 6N5, Canada

(*Received* 12 *April* 1996 *and in final form* 1 *August* 1996)

Abstract—A two-fluid model was developed to predict the wall temperature of a tube during inverted-annular film-boiling (IAFB). This model correctly accounts for the effects of flow variables such as mass flux, inlet subcooling, heat flux and pressure. The relations for shear stress and heat transfer rates are the major components in this model. A unique methodology is utilized to derive these relations. Comparisons between the two-fluid model predictions and experimental data from four fluids (water, Freon-12, Freon-22, and Freon-134a) show good agreement over a wide range of flow conditions. The comparisons resulted in overall root-mean-square (RMS) errors of 14.90, 5.67, 6.58 and 6.19% with the data of water, Freon-12, Freon-22 and Freon-134a, respectively. The model shows better performance than other IAFB prediction methods that were assessed during the course of this study.

1. INTRODUCTION

Flow film boiling is generally divided into inverted annular film boiling (IAFB), encountered at low qualities (usually at void fractions below 50%), and dispersed flow film boiling (DFFB), encountered at high qualities (void fractions beyond 80%). IAFB is characterized by high surface temperatures and consists of a continuous liquid core at the centre of the channel, surrounded by a vapour blanket covering the heated surface. DFFB is characterized by a moderate surface temperature increase and consists of a continuous vapour core with entrained liquid droplets. The DFFB regime can also be created from the break-up of the liquid core downstream of the IAFB regime. Depending on the flow conditions, thermal non-equilibrium between vapour and liquid can be a significant factor and can result in a high vapour superheat. A transition region with churns of liquid (in various sizes) flowing in the vapour core is anticipated at void fractions between 50 and 80%. It is a highly unstable region that has not been studied in detail.

Film boiling heat transfer is important in the safety analysis of postulated loss-of-coolant accidents (LOCAs) of water-cooled nuclear reactors: during a LOCA, a portion of the fuel bundle can experience film boiling. Film boiling could also occur during a loss-of-regulation accident (LORA), where the reactor power accidentally increases. Therefore, the film boiling regime is important in reactor safety studies, as it is during this boiling mode that high fuel sheath temperatures are usually encountered and that burnout may occur. Also, the post-CHF regime is of considerable practical interest in many other applications, such as steam generators, evaporators, cryogenic systems and metallurgical processing.

A number of heat transfer prediction methods have been suggested for both IAFB and DFFB. They vary from simple correlations considering only the single-phase heat transfer from the heated surface to vapour [1–3], to sophisticated two-fluid models that account for the detailed heat transfer mechanisms from the heated surface to both the liquid and vapour phases [4–6]. In many cases, however, these prediction methods are valid only for conditions within their respective data base and cannot be extended. Hammouda [7] reviewed and assessed several prediction methods using data from this study and data from the Chalk River Laboratories (CRL) data bank [8–10]. Both the prediction accuracy and the parametric

† Author to whom correspondence should be addressed.

NOMENCLATURE

A	area [m^2]
C_p	specific heat capacity at constant pressure [$Jkg^{-1} K^{-1}$]
D	tube diameter [m]
D_h	equivalent hydraulic diameter [m]
d	droplet diameter [m]
g	acceleration due to gravity [ms^{-2}]
G	mass flux [$kgm^{-2} s^{-1}$]
h	heat transfer coefficient [$Wm^{-2} K^{-1}$]
h_{fg}	latent heat of vaporization [Jkg^{-1}]
h_l	enthalpy of subcooled liquid [Jkg^{-1}]
h_g	enthalpy of saturated vapour [Jkg^{-1}]
h_v	enthalpy of superheated vapour [Jkg^{-1}]
k	thermal conductivity [$Wm^{-1} K^{-1}$]
Nu	Nusselt number
P	pressure [Pa]
P_i	interfacial perimeter [m]
Pr	Prandtl number
P_w	heated wall perimeter [m]
q	heat flux [Wm^{-2}]
R	tube radius [m]
Re	Reynolds number
t	temperature [°C]
U	velocity [ms^{-1}]
U_r	relative velocity between vapour and liquid [ms^{-1}]
W	mass flow rate [kgs^{-1}]
W'	rate of liquid evaporation per unit length [$kgm^{-1} s^{-1}$]
W''	rate of liquid evaporation per unit area [$kgm^{-2} s^{-1}$]
x	flow quality (vapour weight fraction)
z	axiai distance from inlet [m].

Greek

α	void fraction
δ	vapour film thickness [m]
ε	emissivity
μ	viscosity [Nsm^{-2}]
ρ	density [kgm^{-3}]
σ	Stefan–Boltzman constant ($=5.6697 \times 10^{-8}$) [$Wm^{-2} K^{-4}$]
τ	shear stress [Nm^{-2}].

Subscripts

CHF	critical heat flud
DNB	departure from nucleate boiling
eq	equilibrium
f	saturated liquid
g	saturated vapour
hom	homogeneous
i	interface
i–l	interface to liquid
l	subcooled liquid
rad	radiation
sat	saturation
v	superheated vapour
vf	at film temperature
v–i	vapour to interface
w	wall
w–i	wall to interface.

trends of these methods are examined over a wide range of flow conditions, particularly at medium-to-high pressures and moderate-to-high mass fluxes. None of the existing models and correlations is able to adequately predict the heated surface temperature for all flow conditions. In general, phenomenological models provide worse prediction accuracy than the empirical correlations. This is mainly caused by the limited applicability of the constitutive relations employed within these models.

2. TWO-FLUID MODELLING OF INVERTED ANNULAR FILM BOILING

2.1. *General*

In the present analysis, a new two-fluid model for the IAFB regime is presented, which is based on more general constitutive relations, with a minimum of empirical coefficients. This task has been achieved in this study by deriving simple relations for mass, momentum and energy transfer based on the physical phenomena involved.

2.2. *Methodology*

The approach followed here is to derive the conservation equations for each phase separately. Then, the flow field is completely specified by performing axial integration of the model equations. In general, mathematical modelling of a two-fluid model involves the following:

- conservation equations for mass, momentum, and energy for each phase;
- relevant constitutive relations of mass, momentum and energy transfer; and
- boundary and initial conditions.

The development of constitutive relations is a critical step in a two-fluid model: it is these relations that

distinguish one two-fluid model from another, since the basic conservation equations are usually the same for any two-fluid model.

2.3. *Assumptions*

The mass, momentum and energy equations are derived on the basis of the following assumptions:

(1) The flow is steady.
(2) The flow in the liquid core is turbulent. This assumption is reasonable for high mass flow rates.
(3) The liquid core contains no vapour bubbles. This assumption is reasonable in the subcooled IAFB region. However, some entrainment of vapour into the liquid core may be possible in the saturated IAFB region.
(4) The vapour layer contains no entrained liquid. This is more likely to be true for the subcooled IAFB region, where the interface is relatively smooth.
(5) Thermodynamic non-equilibrium holds for the complete IAFB regime.
(6) The vapour film flow is turbulent for vapour Reynolds numbers, Re_v, larger than 100 and laminar otherwise. It has been shown by Hsu and Westwater [11] that transition to turbulent flow in the vapour film occurs at an Re_v value of 100.
(7) The interfacial velocity, U_i, is equal to the liquid average velocity, U_l.
(8) The vapour–liquid interface is at saturation.
(9) Direct liquid–wall contact does not occur during film boiling.
(10) Liquid flows in the centre of the flow channel and is separated from the heated wall by a thin vapour film.
(11) The vapour film thickness is very small with respect to the tube radius (which will usually be the case). Therefore, the vapour is treated as flow between two parallel plates, the heated wall and the liquid–vapour interface. This allows the use of a cartesian coordinate system, instead of a cylindrical coordinate system.

2.4. *Conservation equations*

The one-dimensional two-fluid equations relevant to the IAFB regime can be readily obtained from the general two-phase flow equations [12–16]. However, Hammouda [7] has rederived these equations directly using the previous assumptions and they are given below:

$$\frac{d}{dz}[\rho_v \alpha U_v] = \frac{W'}{A} \tag{1}$$

$$\frac{d}{dz}[\rho_l (1-\alpha) U_l] = -\frac{W'}{A} \tag{2}$$

$$-\alpha\frac{dP}{dz} - g\rho_v\alpha - \frac{\tau_i P_i}{A} - \frac{\tau_w P_w}{A} = \rho_v \alpha U_v \frac{dU_v}{dz} + \frac{W'}{A}[U_v - U_l] \tag{3}$$

$$-(1-\alpha)\frac{dP}{dz} - g\rho_l(1-\alpha) + \frac{\tau_i P_i}{A} = \rho_l(1-\alpha)U_l\frac{dU_l}{dz} \tag{4}$$

$$\alpha U_v \frac{dh_v}{dz} = \frac{q_{w-v}P_w}{\rho_v A} - \frac{q_{v-i}P_i}{\rho_v A} + \frac{W'(h_g - h_v)}{\rho_v A} \tag{5}$$

$$(1-\alpha)U_l\frac{dh_l}{dz} = \frac{q_{i-l}P_i}{\rho_l A} - \frac{W'(h_f - h_l)}{\rho_l A}. \tag{6}$$

2.3.1. *Other relations.* The vapour layer thickness can be expressed as a function of the tube radius and the void fraction,

$$\delta = R(1-\sqrt{1-\alpha}) \tag{7}$$

and the cross-sectional area, interfacial and inside tube wall peripheral lengths as

$$A = \pi R^2, \quad R = \text{tube radius} \tag{8}$$

$$P_i = 2\pi(R-\delta) \tag{9}$$

$$P_w = 2\pi R. \tag{10}$$

2.5. *Constitutive relations*

2.5.1. *Approach.* This analysis is based on a fundamentally different approach to the problem of providing constitutive relations for two-fluid models of IAFB. It will be shown that this approach works well when applied to systems having several degrees of freedom, which are caused by the thermal and mechanical non-equilibrium between the phases, such as in IAFB. It is not intended to rigorously develop or to demonstrate the overall capability of the proposed relations here, but to show that two-fluid model predictions of heat transfer in the IAFB regime can be based on the concept of reduction of degrees of freedom of the system. This can be achieved by properly identifying and establishing physically sound relationships between the main parameters. For instance, instead of attempting to provide independent equations for the shear stresses at the wall and the interface based on single-phase or adiabatic annular two-phase flow relations, as is usually done in two-fluid models of IAFB, a relationship between the wall shear stress and interfacial shear stress should be developed. Then, it becomes only necessary to provide a single equation for either the shear stress at the wall or at the interface, hence reducing the degrees of freedom of the system.

The present approach has not been offered previously to describe the hydrodynamics and heat transfer in the IAFB regime. In the following sections, closure relations for the various heat transfer and shear stress components are proposed in order to complete the one-dimensional two-fluid model of the IAFB.

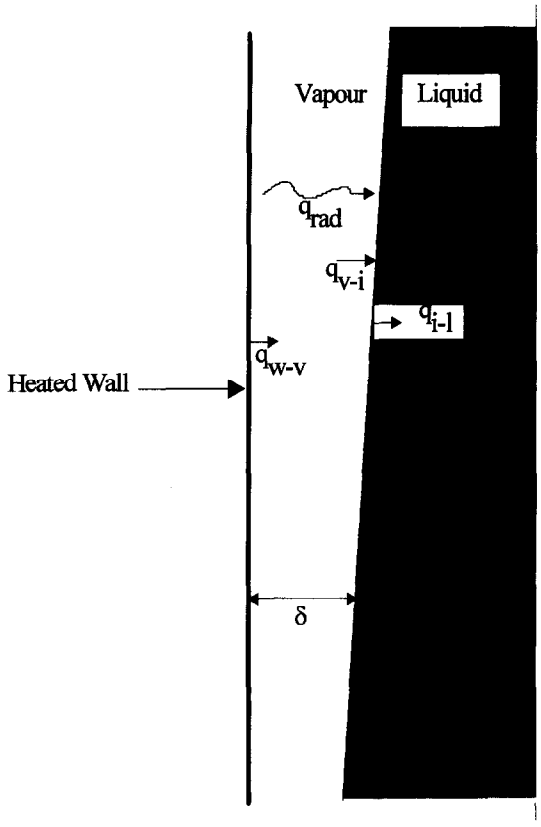

Fig. 1. Heat flux components in IAFB.

2.5.2. *Heat flux*. The heat transfer process in IAFB is a three-step process: heat transfer from wall-to-vapour (q_{w-v}), from vapour-to-interface (q_{v-i}), and from interface-to-liquid core (q_{i-l}). The heat transfer components q_{w-v}, q_{v-i}, and q_{i-l} are schematically shown in Fig. 1. One main limitation of two-fluid models of IAFB is the large degree of uncertainty involved in specifying relations for the heat transfer components. In most two-fluid models, single-phase convective heat transfer correlations are often used to evaluate the heat transfer components q_{w-v}, q_{v-i} and q_{i-l}. These empirical equations are usually independently developed for single-phase flow situations and there is often little justification for their application to a two-phase flow situation, such as IAFB. As a result, they give frequently questionable heat transfer predictions, when applied to IAFB. As previously noted, the current approach will attempt to provide physically sound relationships between q_{w-v}, q_{v-i} and q_{i-l} thus reducing the number of degrees of freedom in the system.

A number of these relations can be readily obtained based on the conservation of energy:

$$Q_w = q_w P_w = q_{w-v} P_w + q_{rad} P_w \tag{11}$$

$$Q_v = q_{w-v} P_w - q_{v-i} P_i \tag{12}$$

$$Q_{ev} = q_{ev} P_i = q_{v-i} P_i + q_{rad} P_w - q_{i-l} P_i \tag{13}$$

where Q_w, Q_v and Q_{ev} are the wall heat transfer rate, vapour heating rate and evaporation heat transfer rate per unit axial length, respectively. Equation (11) simply states that the heat transfer mechanism from the wall is by wall-to-vapour convection and wall-to-liquid radiation (q_{rad}). Equation (12) expresses the vapour heating source, Q_v, causing superheating of the vapour phase. Equation (13) states that the total heat transfer to the liquid is used partially for evaporation at the interface and partially for reduction of subcooling in the liquid core.

Equations (11)–(13) are derived on the basis of first principles; other relations between q_{w-v}, q_{v-i} and q_{i-l} can be derived based on phenomenological reasoning of the heat transfer process that satisfies thermodynamic limits. For steady-state conditions, the predicted heat fluxes q_{w-v}, q_{v-i} and q_{i-l} must satisfy the following thermodynamic limits:

$$\frac{q_{v-i} P_i}{q_{w-v} P_w} \leqslant 1 \tag{14}$$

$$\frac{q_{i-l} P_i}{q_{v-i} P_i + q_{rad} P_w} \leqslant 1 \tag{15}$$

$$\frac{q_{i-l} P_i}{q_{w-v} P_w + q_{rad} P_w} \leqslant 1. \tag{16}$$

Hammouda [7] has noted that many of the current IAFB models do not satisfy these limits for certain flow conditions; such as high subcooling, or high mass flux. This is primarily due to the limited range of validity of the empirical constitutive relations used.

(a) Relation for q_{v-i}/q_{w-v}.

The ratio of heat transfer rates from wall-to-vapour (q_{w-v}) and from vapour-to-interface (q_{v-i}), q_{v-i}/q_{w-v}, may be expressed as follows:

$$\frac{q_{v-i}}{q_{w-v}} = \left(\frac{h_{v-i}}{h_{w-v}}\right)\left(\frac{T_v - T_{sat}}{T_w - T_v}\right). \tag{17}$$

For turbulent flow in the vapour, the heat transfer coefficients, h_{w-v} and h_{v-i}, are directly dependent on the Reynolds numbers, Re_{w-v} and Re_{v-i} and the Prandtl numbers, Pr_{w-v} and Pr_{v-i}. Therefore, the ratio h_{w-v}/h_{v-i} must also be dependent on these dimensionless numbers. By definition, the Re_{w-v} and Re_{v-i} can be expressed as follows:

$$Re_{w-v} = \frac{\rho_v U_v 2\delta}{\mu_v}$$

$$Re_{v-i} = \frac{\rho_v |U_v - U_l| 2\delta}{\mu_v} \tag{18}$$

and Pr_{w-v} and Pr_{v-i} as

$$Pr_{w-v} = \frac{\mu_v Cp_v}{k_v} = Pr_{v-i} \tag{19}$$

thus ignoring property differences caused by different temperatures in the wall–vapour boundary and vapour-interface boundary layer. Next, it is assumed that

h_{w-v} and h_{v-i} take a similar functional form as that of the Dittus–Boelter relation [17], such that

$$h_{w-v} = \frac{k_v}{2\delta} C_{w-v} Re_{w-v}^m Pr_{w-v}^n$$

$$h_{v-i} = \frac{k_v}{2\delta} C_{v-i} Re_{v-i}^m Pr_{v-i}^n \quad (20)$$

and the ratio (h_{v-i}/h_{w-v}) becomes

$$\frac{h_{v-i}}{h_{w-v}} = \frac{C_{v-i}}{C_{w-v}} \left(\frac{U_v - U_l}{U_v} \right)^m. \quad (21)$$

The heat transfer near the vapour–liquid interface is considerably enhanced due to interfacial waves and turbulence. Hence, the coefficient C_{v-i} is expected to be higher than C_{w-v}. However, since U_v is greater than $(U_v - U_l)$, this is assumed to compensate for the higher values of C_{v-i}. Therefore, this implies that h_{w-v} and h_{v-i} are of the same order of magnitude and that the ratio h_{v-i}/h_{w-v} is assumed to approach one (see also Section 4 for further discussion). This means that q_{v-i}/q_{w-v} is predominantly controlled by the temperature difference ratio and

$$\frac{q_{v-i}}{q_{w-v}} \cong \frac{T_v - T_{sat}}{T_w - T_v}. \quad (22)$$

The lower limit of the heat transfer rate from wall-to-vapour, q_{w-v}, is that of pure conduction through a vapour film of thickness δ with the vapour temperature evaluated at the average value between wall and saturation temperatures (film temperature):

$$T_{vf} = \frac{T_w + T_{sat}}{2}. \quad (23)$$

This results in $q_{w-v} = q_{v-i}$ in equation (22). However, because of evaporation, the value of the vapour temperature is lower than the value of the film temperature $((T_v - T_{sat})/(T_w - T_v) < 1)$. This is significant in that it influences the value of the thermophysical properties of the vapour. The upper limit of the heat transfer rate from the vapour-to-interface, q_{v-i}, is restricted by the thermodynamic limit (equation (14)), such that

$$q_{v-i} P_i = q_{w-v} P_w. \quad (24)$$

(b) Relation for $(q_{v-i} + q_{rad})/q_{i-l}$.

The ratio $(q_{v-i} + q_{rad})/q_{i-l}$ can be treated in a similar manner as in Section (a), namely

$$\frac{q_{v-i} + q_{rad}}{q_{i-l}} = \frac{h_{v-i}(T_v - T_{sat})}{h_{i-l}(T_{sat} - T_l)} + \frac{h_{rad}(T_w - T_{sat})}{h_{i-l}(T_{sat} - T_l)}. \quad (25)$$

Equation (25) can be rewritten as

$$\frac{q_{v-i} + q_{rad}}{q_{i-l}} = \Phi_1 \frac{T_v - T_{sat}}{T_{sat} - T_l} + \Phi_2 \frac{T_w - T_{sat}}{T_{sat} - T_l} \quad (26)$$

where

$$\Phi_1 = \frac{h_{v-i}}{h_{i-l}} \quad (27)$$

and

$$\Phi_2 = \frac{h_{rad}}{h_{i-l}}.$$

Expressions for these two parameters will be given shortly. Due to equations (22) and (26), only a reliable equation for q_{w-v} is needed to determine q_{v-i} and q_{i-l}. This will be the focus of the next section.

(c) Heat transfer from the wall, q_{w-v}.

There are two choices for providing an equation for q_{w-v}: (i) to use a single-phase vapour equation or (ii) to develop a heat transfer equation based on IAFB data. The latter is very difficult to achieve, since it requires measurements of actual vapour temperatures for a wide range of flow conditions. The former, however, is easier to implement, as long as modifications for two-phase flow conditions are included and, hence, it is adopted here. Probably the best-suited single-phase equations for q_{w-v} in the IAFB regime are those derived for the concentric annulus geometry, because of the close geometrical resemblance of the vapour flow cross-sectional area and flow in a concentric annulus. In that respect, Kays' [18] equations for heat transfer rates in a concentric annulus are applicable for a wide range of flow conditions.

For flow between parallel planes, Kays gives the following expression:

$$q_{w-v} = \frac{k_v Nu_v}{2\delta} \frac{(T_w - T_v)}{1 - \frac{q_{v-i}}{q_{w-v}} \theta} \quad (28)$$

where Nu_v is the Nusselt number and θ the influence coefficient. For laminar flow between two parallel planes, Nu_v and θ are given by $Nu_v = 5.385$ and $\theta = 0.346$. for turbulent flow between two parallel planes, Kays gives Nu_v and θ in tabular form up to a Reynolds number of 10^6 and Prandtl numbers from 0 to 1000.

In this study, equation (28) is modified to account for the difference between flow between parallel planes and the vapour flow in the vapour layer of the IAFB regime. Note that the boundary condition of a fluid-to-fluid, instead of fluid-to-wall, may play an important role in affecting the turbulence structure near the interface, because of the complex wave patterns at the liquid–vapour interface, which present some sort of roughness to the vapour flow.

Equation (28) can be solved by substituting equation (22) for q_{v-i}/q_{w-v} and using equation (7) for δ, as follows:

$$q_{w-v} = \frac{Nu_v}{\left[1 - \frac{T_v - T_{sat}}{T_w - T_v} \theta\right] D[1 - \sqrt{1-\alpha}]} \frac{k_v}{} (T_w - T_v). \quad (29)$$

After substituting equation (29) in equation (22), an expression for h_{v-i} can be written as

$$h_{v-i} = \frac{Nu_v}{\left[1 - \dfrac{T_w - T_v}{T_v - T_{sat}}\theta\right]} \frac{k_v}{D[1-\sqrt{1-\alpha}]}. \quad (30)$$

Next, h_{i-l} is expressed as

$$h_{i-l} = 0.023 \frac{k_l}{D\sqrt{1-\alpha}} Re_l^{0.8} Pr_l^{0.4} F. \quad (31)$$

This is basically the Ditus–Boelter equation for the heat transfer coefficient for turbulent flow in a circular tube of radius $(R-\delta)$ subjected to a constant-temperature boundary condition (T_{sat} in this case). The parameter F is introduced to approximately account for entrance-length effects and is given as

$$F = 1 + 1.4\frac{R}{z}. \quad (32)$$

In equation (31) the liquid velocity U_l is employed for calculating h_{i-l}, since using $(U_l - U_i)$ gives zero values for h_{i-l}, because of the assumption of $U_i = U_l$. This method is similar to that of Analytis and Yadigaroglu [4]. This approach may not seem logical, but the results are not strongly affected by this assumption, as will be shown later in Section 4. Further, Analytis and Yadigaroglu argue that the interfacial velocity can be determined only by solving the two-dimensional Navier–Stokes equations in the liquid and the vapour phases, a difficult task that is further complicated by a turbulent-flow entrance-length problem.

By assuming that the vapour film is transparent and that the wall is grey, the radiation heat flux to the liquid core interface q_{rad} can be expressed as

$$q_{rad} = \frac{\sigma(T_w^4 - T_{sat}^4)}{\dfrac{1}{\varepsilon_w} + \dfrac{1}{\varepsilon_l\sqrt{1-\alpha}} - 1}. \quad (33)$$

thus the radiation heat transfer coefficient h_{rad} is

$$h_{rad} = \frac{\sigma(T_w^4 - T_{sat}^4)}{\left(\dfrac{1}{\varepsilon_w} + \dfrac{1}{\varepsilon_l\sqrt{1-\alpha}} - 1\right)(T_w - T_{sat})}. \quad (34)$$

From equations (30), (31) and (34), approximate expressions for Φ_1 and Φ_2 can be obtained as

$$\Phi_1 = \frac{Nu_v}{\left[1 - \dfrac{T_w - T_v}{T_v - T_{sat}}\theta\right]} \frac{k_v}{k_l} \frac{\sqrt{1-\alpha}}{(1-\sqrt{1-\alpha})} \frac{1}{0.023F} Re_l^{-0.8} Pr_l^{-0.4}$$

$$\Phi_2 = \frac{\sigma(T_w^4 - T_{sat}^4) D\sqrt{1-\alpha}}{0.023 F k_l \left(\dfrac{1}{\varepsilon_w} + \dfrac{1}{\varepsilon_l\sqrt{1-\alpha}} - 1\right)(T_w - T_{sat})} Re_l^{-0.8} Pr_l^{-0.4}. \quad (35)$$

In applying the model, it was found that: (i) the ratio q_{rad}/q_{i-l} is very small compared to q_{v-i}/q_{i-l}, except at extremely high wall temperatures; and (ii) the model predictions are not very sensitive to the h_{v-i}/h_{i-l} ratio (see Section 4), except probably near the CHF location and at very high inlet subcoolings and low heat fluxes. Thus a value of one for Φ_1 was chosen, since, in general, it gives the best prediction accuracy for most of the flow conditions examined. This implies that q_{v-i}/q_{i-l} is strongly controlled by the temperature difference ratio. Consequently, it is decided to simplify equation (26) to the following form

$$\frac{q_{i-l}}{q_{v-i}} = \frac{T_{sat} - T_l}{T_v - T_{sat}} \quad (36)$$

which is very similar to the form of equation (22). Although equation (36) appears to be too simple, it provides a reasonably accurate prediction of the model. In addition, it has the advantage of being free of empirical factors that might need tuning to different data sets.

(d) Vapour generation.

For the vapour generation per unit axial length, W', the following expression is given

$$W' h_{fg} = q_{ev} P_i \quad (37)$$

where the evaporation heat flux q_{ev}, can be written as

$$q_{ev} P_i = q_{v-i} P_i + q_{rad} P_w - q_{i-l} P_i. \quad (38)$$

2.5.3. *Shear stress.* In general, interfacial and wall shear stresses are expressed in terms of friction factors, which can be obtained by solving the Navier–Stokes equations in the vapour film and in the liquid core or extrapolated from the shear stress correlations in the annular flow regime.

(a) Interfacial shear stress.

The liquid–vapour interface in the IAFB regime may be smooth or wavy, depending on the film thickness and the mass flux. Accounting for wave effects may not be easy or practical for an IAFB model; hence, IAFB two-fluid models are often based on the assumption that the liquid–vapour interface is smooth, and single-phase shear stress relations are applicable. In general, interfacial shear stress in the IAFB for a wavy interface will be higher than for a smooth vapour–liquid interface, due to the hydrodynamic drag of interfacial waves (similar to the roughness effect). Therefore, correction factors are often introduced to account for this effect. The constitutive relation for τ_i can be expressed in terms of a friction factor, as is done in single-phase flow:

$$\tau_i = \frac{f_i \rho_v U_r |U_r|}{2} \quad (39)$$

where U_r is the relative velocity at the interface. However, no data are available to allow calculation of f_i, and if τ_i is expressed in terms of f_i, correction factors, usually referred to as enhancement factors, are used with this equation. These enhancement fac-

tors are tuned to fit a particular data set, thus limiting the range of applicability of the models to the range of the data base from which these factors are derived. Instead, since the momentum interaction between the phases is directly affected by the wall shear stress through the interfacial shear, it is assumed that a specific relationship between τ_w and τ_i expressing this physical mechanism is present.

A relationship between τ_i and τ_w can be approximated from consideration of the momentum equation of the vapour phase. From equation (3), the equation for the interfacial shear is

$$\frac{\tau_i P_i}{A} = -\alpha\frac{dP}{dz} - g\rho_v\alpha - \frac{\tau_w P_w}{A} - \rho_v\alpha U_v\frac{dU_v}{dz} + \frac{W'(U_l - U_v)}{A}. \quad (40)$$

This equation is the basic equation for the evaluation of τ_i, but it needs to be simplified to facilitate the handling of this equation. The most straightforward assumption is to assume constant shear stress, equal to the wall shear stress, within the vapour film. This would be a good approximation when the vapour film is very thin and τ_i very high in comparison to the gravitational, accelerative and pressure gradient forces exerted on the film. These conditions can be closely satisfied in the subcooled IAFB region, where the vapour generation rate is very low and the acceleration term is small.

The model predictions, however, should be expected to deviate from the data in the saturated and agitated IAFB regions, where the vapour generation rate is high (thicker vapour film) and the acceleration term in equation (40) may become dominant. Nevertheless, Cachard [5] has shown that this term is negligible, even with significant vaporization. Thus, it is assumed that

$$|\tau_i| \cong |\tau_w|. \quad (41)$$

(b) Wall shear stress.

Assuming turbulent flow in the vapour film, any wall shear stress relation in single-phase vapour flow can be used to find τ_w. Therefore, empirical equations derived for friction coefficients in turbulent flow in tubes can be employed, provided that some kind of equivalent tube diameter could be defined for evaluating the Reynolds number. The usual practice is to use the hydraulic diameter, which for flow between parallel plates (the wall and the interface) reduces to

$$D_h = 2\delta \quad (42)$$

where δ is the vapour film thickness given by equation (7). The wall shear stress is then expressed as follows:

$$\tau_w = \frac{f_w}{2}\rho_v U_v|U_v|. \quad (43)$$

During this study, equations for the friction factor, f_w, recommended by Bhatti and Shah [19] were examined. It was found that the model gives best prediction accuracy with the following equation.

$$f_w = (1 + 0.0925r^*)f_c \quad (44)$$

where

$$\frac{1}{\sqrt{f_c}} = 1.7372\ln\left(\frac{Re_v}{1.964\ln(Re_v) - 3.8215}\right)$$

$$5\times10^3 \leqslant Re_v \leqslant 10^7$$

and

$$r^* = \frac{R_i}{R} = \frac{R(1-\alpha)^{1/2}}{R} = (1-\alpha)^{1/2}$$

$$Re_v = \frac{\rho_v U_v D_l}{\mu_v}.$$

This equation is due to Bahatti and Shah [19], and for turbulent flow in concentric annuli based on the laminar equivalent diameter, D_l, in the definition of Re_v defined as

$$\frac{D_l}{D_h} = \frac{1 + r^{*2} + \dfrac{(1-r^{*2})}{\ln(r^*)}}{(1-r^*)^2}. \quad (45)$$

For $Re_v < 5\times10^3$ or $Re_v > 10^7$, the following expression is used:

$$f_w = \frac{0.085}{Re_{w-v}^{0.25}} \quad (46)$$

where Re_{w-v} is defined by equation (18). Analytis and Yadigaroglu [4] used equation (46) in their model to calculate f_w. For laminar flow between parallel plates (the wall and the interface), f_w is expressed as

$$f_w = \frac{24}{Re_{w-v}}. \quad (47)$$

The constitutive relations for the IAFB model are summarized in Table 1. Note that these relations have not been refined, since it is the intent to demonstrate the adequacy of this modelling approach, which emphasizes the correct physics combined with a minimum amount of empiricism.

The numerical solution of the model equations is separated into three steps:

(i) the momentum and mass equations are solved for the flow variables (i.e. the velocities, pressure and void fraction);

(ii) the energy equation are solved for the temperature of the vapour and the liquid phases;

(iii) the inside wall temperature is obtained by iteration.

Hence given the initial conditions, the steady-state solution involves a process of direct matrix and iteration solutions at each step. Equations (1)–(6) form a system of ordinary differential equations (ODEs). They are solved as an initial value problem in z-direction using a fourth-order Runge–Kutta method and

Table 1. Summary of constitutive relations used with the present IAFB model

Relations	Equations	Comments
Wall heat transfer	$q_w P_w = q_{w-v} + q_{rad} P_w$	
Wall-to-vapour heat transfer	$q_{w-v} = \frac{Nu_v}{\left[1 - \frac{T_v - T_{sat}}{T_w - T_v}\theta\right] D[1-\sqrt{1-\alpha}]} \frac{k_v}{}(T_w - T_v)$	Modified Kays' equations [18] for flow between parallel planes
	$Nu_v = \frac{5.071}{Pr_v^{0.0439}} + 0.0028 Pr_v^{0.645} Re_v$	
	$\theta = 0.3476 Pr_v^{0.0026} - \frac{0.146 Pr_v^{0.5418} Re_v}{9900}$	
Vapour-to-interface heat transfer	$q_{v-i} = \frac{T_v - T_{sat}}{T_w - T_v} q_{w-v}$	For laminar flow ($Re_v < 100$), conduction across the vapour film is assumed and $q_{v-i} = q_{w-v}$
Wall-to-liquid radiation	$q_{rad} = \frac{\sigma(T_w^4 - T_{sat}^4)}{\frac{1}{\varepsilon_w} + \frac{1}{\varepsilon_l\sqrt{1-\alpha}} - 1}$	Siegel and Howell [20]
Interface-to-liquid heat transfer	$q_{i-l} = q_{v-i} \frac{T_v - T_{sat}}{T_{sat} - T_l}$	
Vaporization heat flux	$q_{ev} P_i = q_{v-i} P_i + q_{rad} P_w - q_{i-l} P_i$	
Interfacial mass transfer	$W'' = \frac{q_{ev} P_i}{h_{fg}}$	
Wall-vapour shear stress	$\tau_w = \frac{f_w}{2} \rho_v U_v^2$	Based on flow between parallel planes.
	Laminar flow: $f_w = \frac{24}{Re_{w-v}}$	
	$Re_{w-v} = \frac{\rho_v U_v 2\delta}{\mu_v}$	
	Turbulent flow: $f_w = (1 + 0.0925 r^*) f_c$	
	$\frac{1}{\sqrt{f_c}} = 1.7372 \ln\left(\frac{Re_v}{1.964 \ln(Re_v) - 3.8215}\right)$	Based on flow in concentric annuli. Bhatti and Shah [19]
	$Re_v = \frac{\rho_v U_v D_l}{\mu_v}$; $r^* = (1-\alpha)^{1/2}$;	
	$D_l = \frac{1 + r^{*2} + \frac{(1-r^{*2})}{\ln(r^*)}}{(1-r^*)^2} 2\delta$	
	For $Re_v < 5 \times 10^3$ or $Re_v > 10^7$: $f_w = \frac{0.085}{Re_{w-v}^{0.25}}$	
Interfacial shear stress	$\tau_i = \tau_w$	
Transition to DFFB regime	$\alpha \geqslant 0.5$	

the initial values of the independent variables specified at the CHF location.

3. COMPARISON WITH MEASUREMENTS

This section compares predictions from the two-fluid model with the data of Hammouda [7] and data from the AECL PDO data base. The results of the comparison are displayed as plots of wall temperature versus thermodynamic equilibrium quality. Also, some of these plots show predictions from the various prediction methods discussed in Hammouda [7], in order to compare them with the new model.

3.1. *Comparison with freon data*

Figure 2 shows a comparison of predicted and measured mass flux effect on the wall temperature distribution at various flow conditions and for two fluids. In general, the model correctly predicts the trend and the magnitude of the wall temperatures. It gives better predictions at low mass flux values. At high mass fluxes, initially, the data has a sharp peak then a steep rapid decrease and then a smooth moderate decrease in wall temperatures downstream. These are the characteristics of the axial wall temperature distribution at high mass flux values, which are discussed in Refs [7, 21]. Initially, the model seems unable to

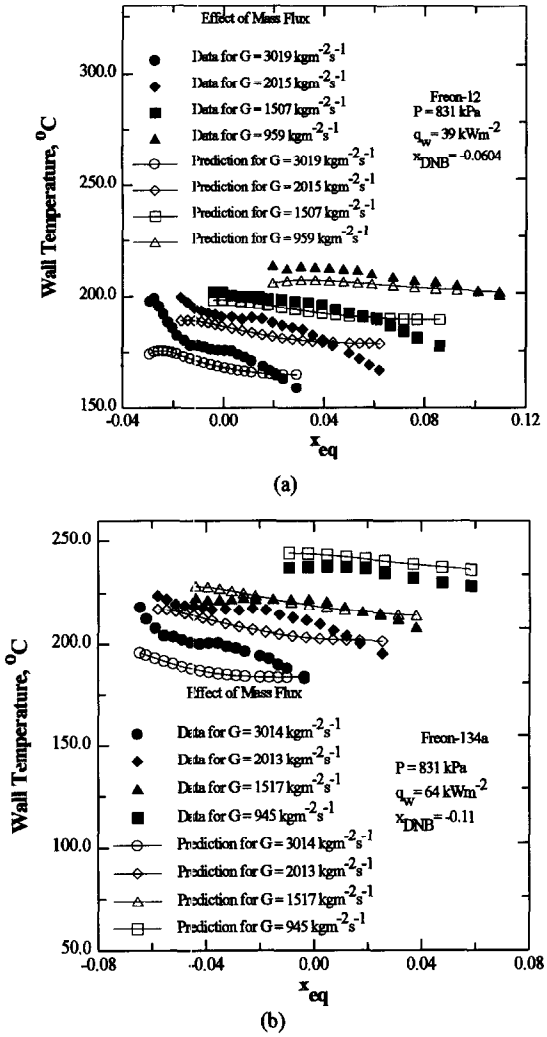

Fig. 2. Comparison of measured mass flux effect with model predictions.

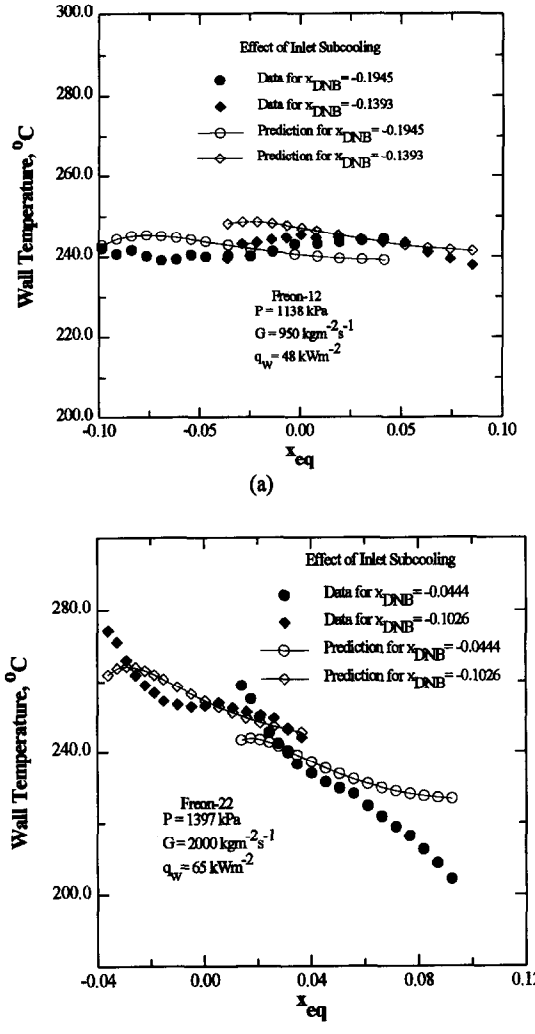

Fig. 3. Comparison of measured inlet subcooling effect with model predictions.

follow the rapid changes in the data, but its prediction accuracy improves as x_{eq} increases. It predicts a lower temperature peak and a lower rate of decrease in wall temperatures at lower x_{eq} values.

Figure 3 shows the effect of inlet subcooling on the wall temperature distribution. Usually the mere effect of inlet subcooling is to shift the T_w vs x_{eq} curves to lower x_{eq} range. The model correctly predicted this trend. Again, as mentioned in the previous section, the model appears to give better agreement with the wall temperature data at lower mass flux values. Figure 4 shows the effect of heat flux on the wall temperature distribution. The model predictions are in good agreement with the data. The data shows that wall temperatures are higher for higher heat fluxes. Figure 5 shows the effect of pressure on the wall temperature distributions. In general, the model correctly predicted the effect of pressure on T_w vs x_{eq}.

In Section 2.5.2, it was argued that h_{w-v} and h_{v-i} are of the same order of magnitude and that the ratio (h_{v-i}/h_{w-v}) approaches one. This assumption has been examined through comparison of model prediction of wall temperatures with experimental data for various values of (h_{v-i}/h_{w-v}). Figure 6(a) clearly shows that the model gives best predictions at (h_{v-i}/h_{w-v}) values approaching one. Figure 6(b) shows root-mean-square (RMS) error distributions vs (h_{v-i}/h_{w-v}) from comparison with 2407 data points of Freon-12 and for a wide range of flow conditions. Note that the results of this comparison are typical of all the model predictions.

For (h_{v-i}/h_{w-v}) values above one, the model tends to underpredict the wall temperatures. This is expected, because a higher heat transfer from vapour-to-interface results in lower vapour superheat (lower T_v), as Fig. 6(a) shows. Since heat transfer from the wall is mainly controlled by convection to the vapour phase, the model underpredicts the data. A similar argument applies to (h_{v-i}/h_{w-v}) values less than one, except this time the model tends to overpredict the data.

Actual data of the ratio (h_{v-i}/h_{w-v}) are not available,

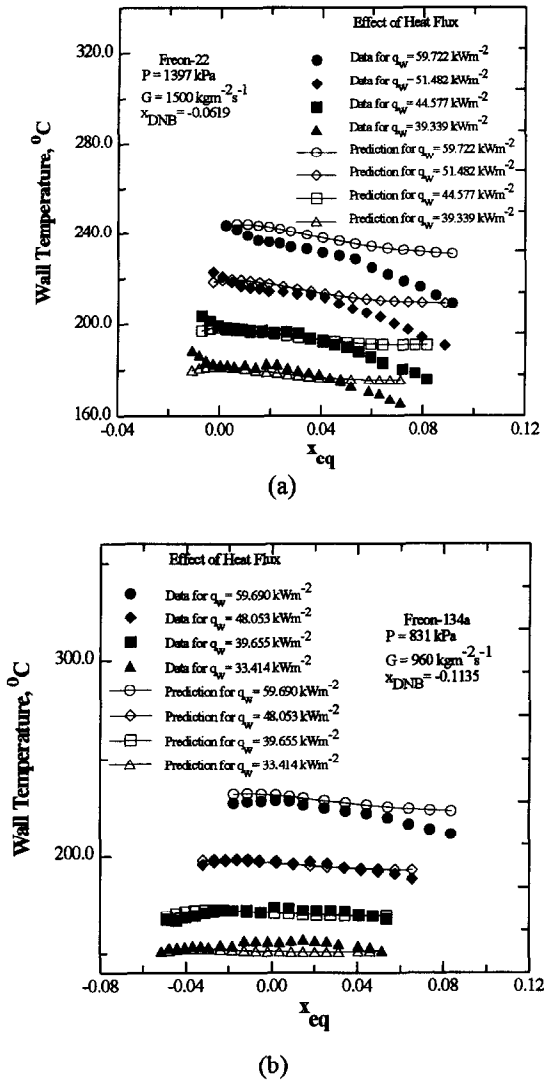

Fig. 4. Comparison of measured heat flux effect with model predictions.

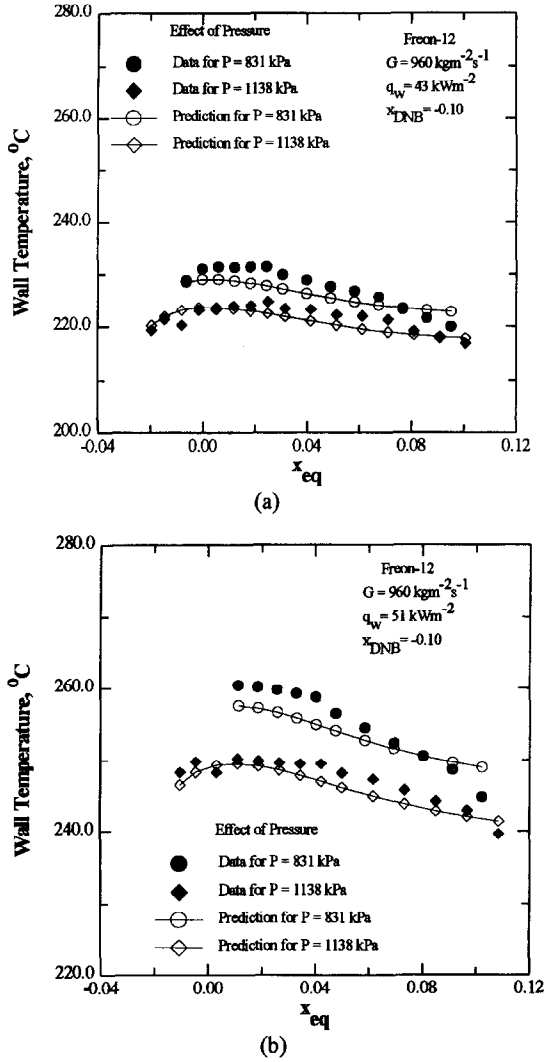

Fig. 5. Comparison of measured pressure effect with model predictions.

due to the experimental difficulty in determining the interfacial heat transfer coefficient, h_{i-l}. Nevertheless, in view of the better agreement obtained between model predictions and data for (h_{v-i}/h_{w-v}) values approaching one, it is reasonable to approximate the ratio of (h_{v-i}/h_{w-v}) to a value of one. It should be cautioned, however, that although this approximation works well within the frame of the present model, it may lead to poor prediction accuracy when applied to other prediction methods, if the actual physical mechanism at the interface leads to values of (h_{v-i}/h_{w-v}) much different from one.

Figure 7 shows the effect of varying the ratio of (h_{i-l}/h_{v-i}) on the model prediction of wall temperatures distribution. The ratio of (h_{i-l}/h_{v-i}) was varied from a value of 0.4–4.0, for the flow conditions shown in Fig. 7. In Fig. 7(a) the maximum value of (h_{i-l}/h_{v-i}) was 9.0, as predicted by equation (31). Figure 7 shows that the impact of changing the values of (h_{i-l}/h_{v-i}) on the wall temperatures distribution is insignificant. In general, the heat transfer from the interface to the liquid core, q_{i-l}, becomes less and less important with increasing x_{eq} values along the heated length of the flow channel, because the bulk liquid core temperature rapidly approaches saturation. Consequently, the contribution of q_{i-l} to the total heat transfer from the wall becomes less significant, except probably near the CHF location and for high inlet subcoolings.

Figures 8 and 9 show prediction of wall temperatures and heat transfer coefficients for three fluids (Freon-12, Freon-134a and Freon-22) and for a wide range of flow conditions. The new model predicts the trend and the magnitude of the data correctly, and it gives much better prediction accuracy than the other prediction methods. In general, the model performs best at lower mass fluxes. At high mass fluxes, none of the prediction methods, including this model, is capable of accurate predictions in the subcooled film boiling region.

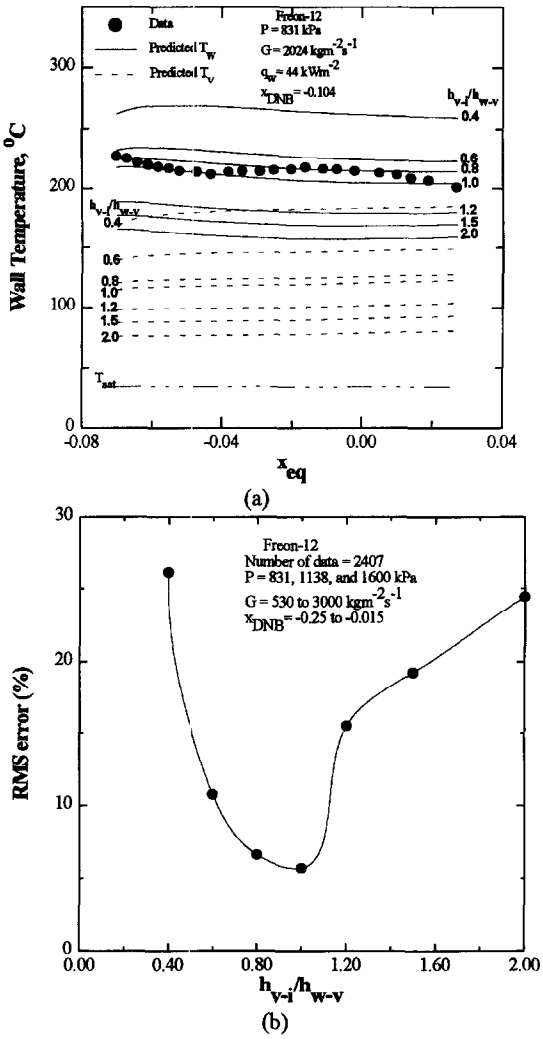

Fig. 6. Deviation of predicted wall temperatures from experimental data of Freon-12 at various values of h_{v-i}/h_w.

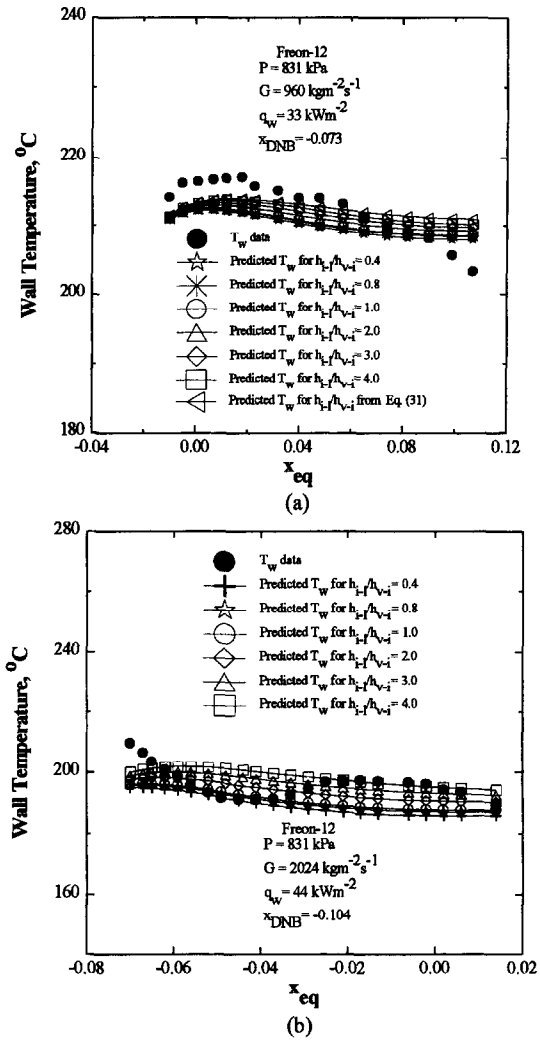

Fig. 7. Model sensitivity to the (h_{i-f}/h_{v-i}) ratio.

3.2. *Comparison with water data*

Figures 10 and 11 show prediction of wall temperatures and heat transfer coefficients for pressure conditions ranging from atmospheric to 10 MPa for water. It is interesting to notice that, in general, the prediction methods have a worse prediction accuracy for the water data than for the refrigerant data of this study.

It is understood that the physical mechanisms of heat transfer in subcooled film boiling are the same for all fluids. Consequently, the greater discrepancies in the predictions for the water data can only be attributed to (i) uncertainties in the water data itself, and (ii) possibly greater importance of radiation. Also, some data sets from different sources, which cover very similar flow conditions, do not agree with each other. Nevertheless, overall the new model still provides the most accurate predictions among the prediction methods examined in this study.

3.3. *Overall comparison*

Table 2 lists the root-mean-square (RMS) and the average errors of the prediction methods examined during this study. The average error and the RMS error are defined as follows.

$$\text{RMS Error} = \left[\frac{1}{n}\sum_{i=1}^{n}(\text{Error})_i^2\right]^{1/2} \tag{48}$$

$$\text{Average Error} = \frac{1}{n}\sum_{i=1}^{n}(\text{Error})_i \tag{49}$$

where Error is a relative error defined as

$$\text{Error} = \frac{\text{Predicted } T_w - \text{Experimental } T_w}{\text{Experimental } T_w} \tag{50}$$

where T_w is the inside tube surface temperature in °C and n is the number of data points. The data of water are from Stewart [9], Laperriere [10] and Fung [8].

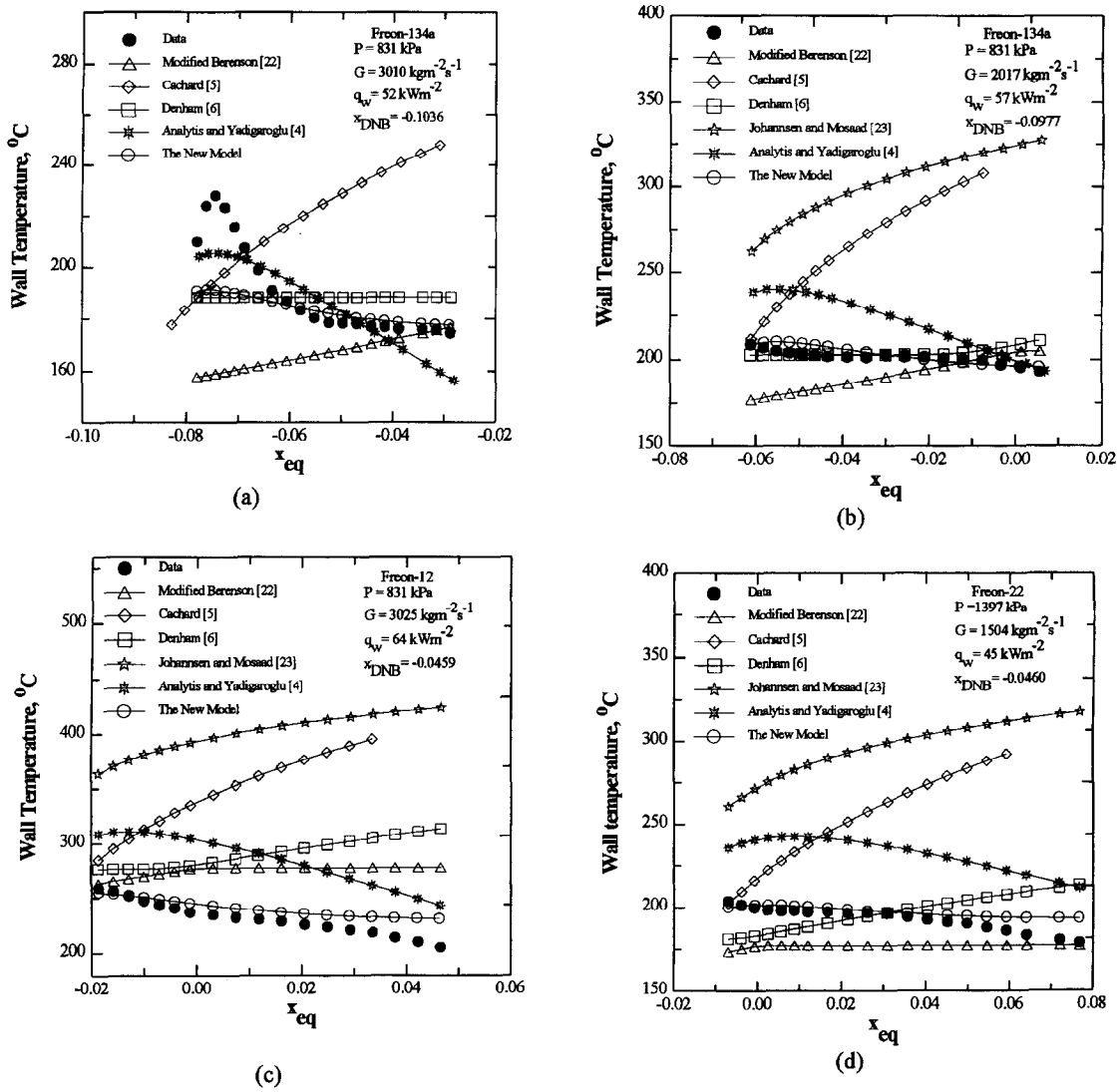

Fig. 8. Comparison of the IAFB model predictions with Freon data.

Overall, for water data, the present model gives conservative predictions of wall temperatures, as indicated by the average error of 5.20%, which has resulted from a total of 2809 data points. Also, the model gives an overall RMS error of 14.88%, which is the lowest. It is of interest to see that the present model provides better prediction accuracy than the modified Berenson correlation [22], which was modified based on the same water data base used for comparison in this study.

For Freon data, the present model gives the lowest RMS errors among all the prediction methods, as Table 2 shows. Overall, the new model yields the lowest RMS errors, and the Johannsen and Mosaad [23] and Cahard [5] models the highest. This is not surprising, since the new model applies to all flow conditions and uses a minimum amount of empiricism, whereas the others contain a large number of empirically determined factors evaluated from water data covering a narrow range of flow conditions.

3.4. *Discussion*

Low quality and subcooled film boiling is of particular interest for the reflood phases of a LOCA. This flow regime usually precedes the arrival of the quench front and influences its rate of progression. As a consequence, the majority of subcooled film boiling prediction methods existing in the literature deal with LOCA conditions at low pressures (up to 0.4 MPa) and low mass fluxes (up to 300 $kgm^{-2}s^{-1}$). The constitutive relations used within these models contain parameters that are approximated (or inferred) from data relevant to LOCA conditions (low pressures and low mass fluxes). This restricts the models to the same conditions. This may explain the poor performance of the prediction methods discussed in Hammouda [7, 24], when compared with the data of this study and to the high-pressure data of water ($P \geqslant 2$ MPa). For example, the Johannsen and Mosaad [23] and Cachard [5] models give very poor prediction accuracy when compared with the moderate-to-high mass flow

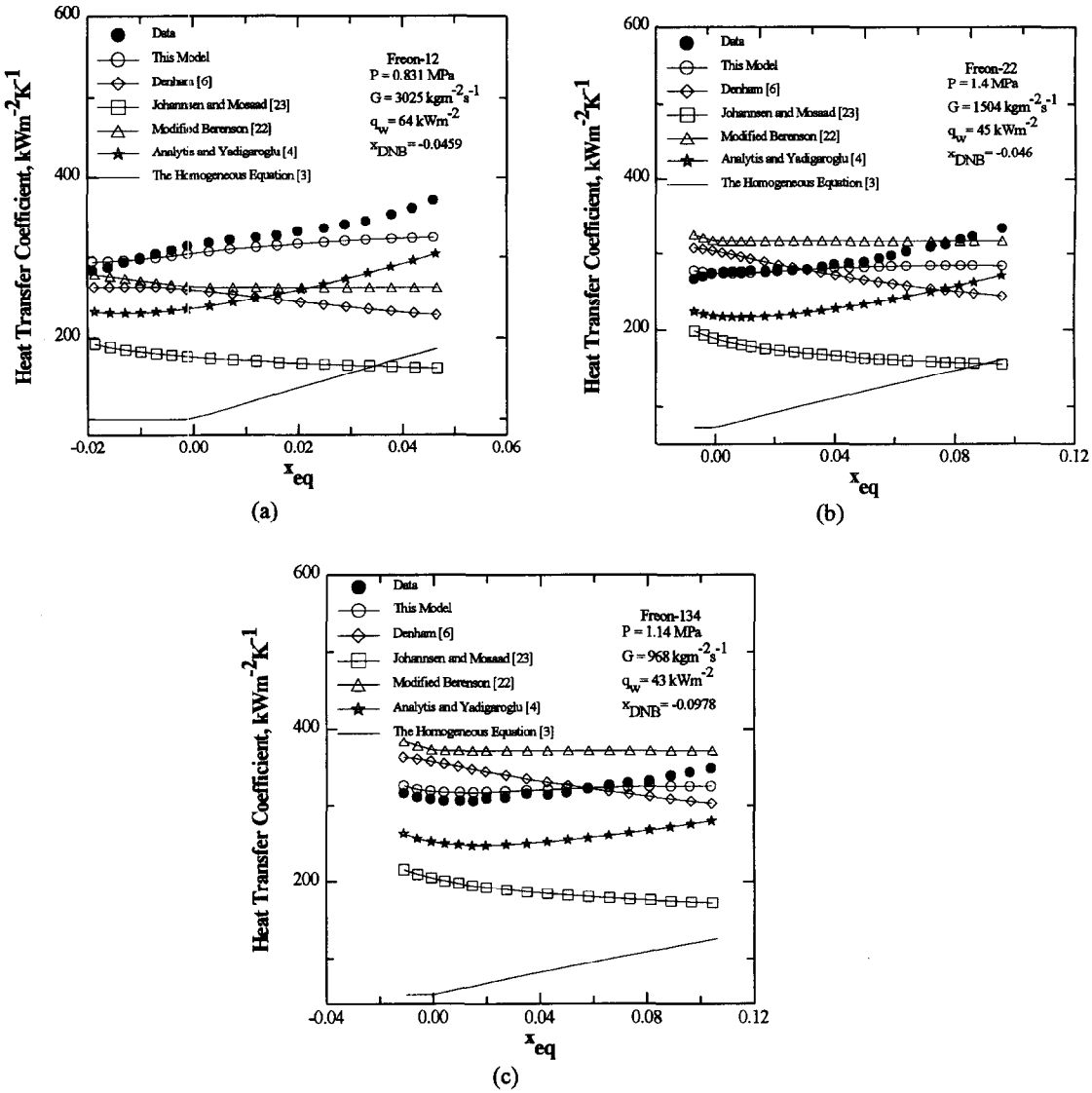

Fig. 9. Comparison of the IAFB model predictions of heat-transfer coefficient with Freon data.

rate and moderate-to-high pressure water data. This is because these models were adjusted to predict heat transfer rates during LOCA conditions. The proposed model does not appear to be limited to low pressure and as is shown by the comparisons.

4. CONCLUSIONS AND FINAL REMARKS

4.1. *Conclusions*

(1) A two-fluid one-dimensional model has been developed to predict the surface temperature of a tube in IAFB at low-to-high pressure and low-to-high flow conditions. This model predictions have been compared with data from four fluids (water, Freon-12, Freon-22 and Freon-134a). The model provides a much better prediction accuracy than other IAFB prediction methods assessed during the course of this study.

(2) The new model is based on a unique methodology of developing constitutive relations. Even though the constitutive relations derived for the new two-fluid model are approximate, it is of interest to see that the method works well in comparison with other methods.

4.2. *Final remarks*

(1) The theoretical model of this study has been developed to demonstrate primarily the adequacy of the modelling approach proposed in Section 2. The constitutive relations employed are based on the simplifying assumptions. Despite this, relatively good agreement has been obtained between model predictions and the data. It is suggested that refinement of these relations should be pursued in the future, to further improve the model predictions.

(2) In highly subcooled film boiling, the vapour film at the heated surface is very thin over most of the IAFB length. All prediction methods, including the

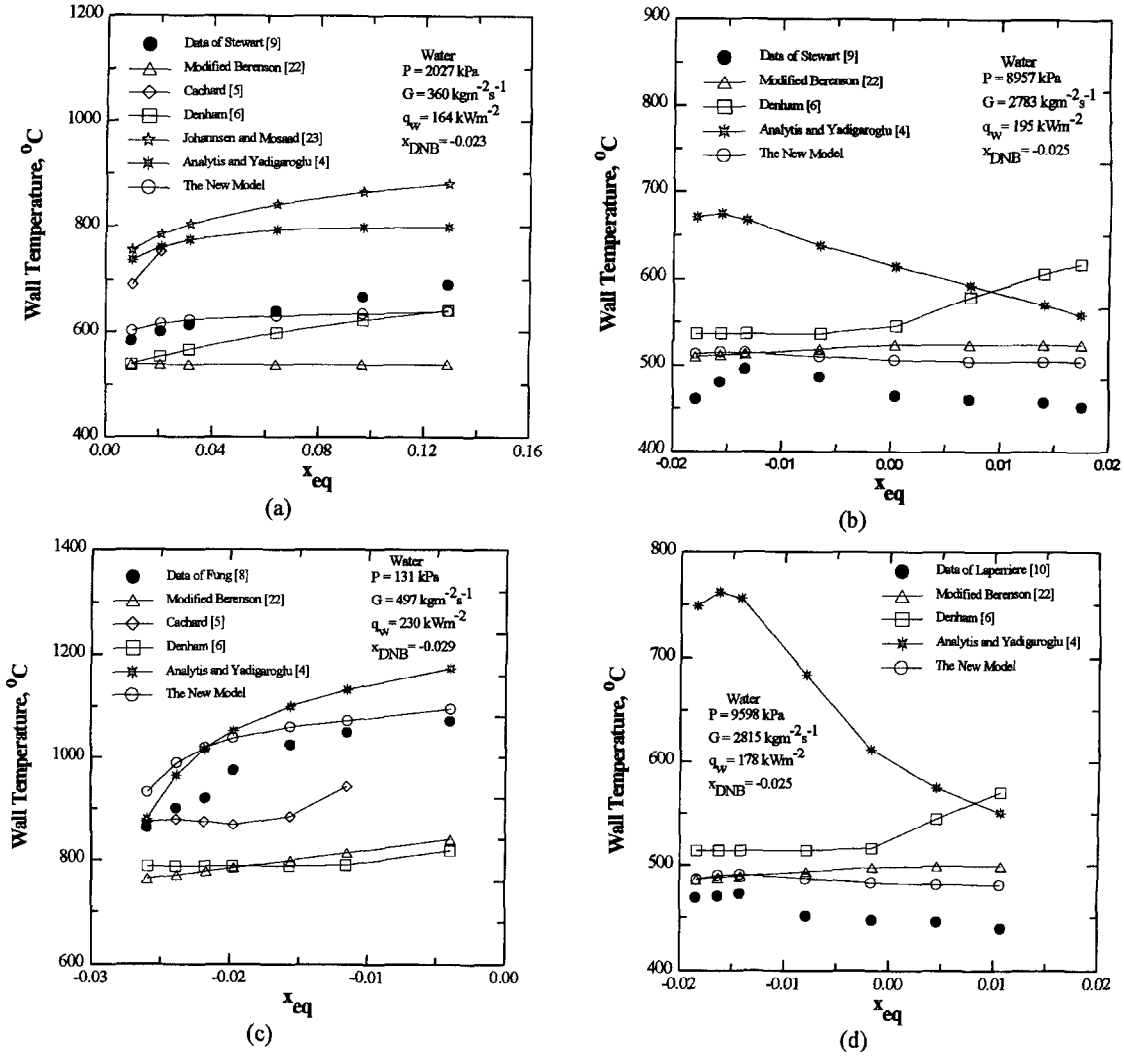

Fig. 10. Comparison of the IAFB model predictions with water data.

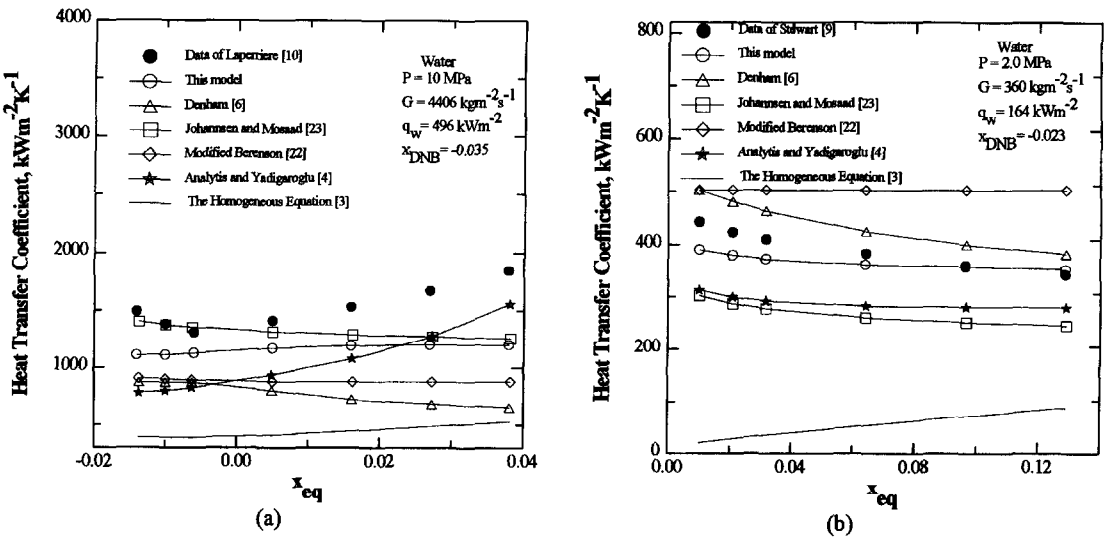

Fig. 11. Comparison of the IAFB model predictions of heat-transfer coefficient with water data.

Table 2. Deviation of predicted wall temperatures from experimental values

Prediction method	RMS%	Average deviation%	Number of data	Fluid
Analytis–Yadigaroglu [4]	21.70	20.44	2407	Freon-12
Denham [6]	16.79	3.54	2407	
Johannsen–Mossad[a] [23]	61.65	56.23	1676	
Modified Berenson [22]	16.94	−7.70	2407	
Cachard [5][a]	34.34	28.24	1518	
New model	5.67	−3.11	2407	
Analytis–Yadigaroglu [4]	19.44	17.96	705	Freon-22
Denham [6]	26.31	11.91	705	
Johannsen–Mosaad[a] [23]	68.22	64.29	481	
Modified Berenson [22]	18.82	−0.81	705	
Cachard[a] [5]	41.57	33.64	309	
New model	6.58	−1.87	705	
Analytis–Yadigaroglu [4]	17.15	11.59	2083	Freon-134a
Denham [6]	15.78	4.55	2083	
Johannsen–Mosaad[a] [23]	70.14	65.87	1172	
Modified Berenson [22]	15.39	−4.07	2083	
Cachard[a] [5]	35.69	31.25	657	
Present model	6.19	−3.14	2083	
Analytis–Yadigaroglu [4]	26.90	19.90	2809	Water
Denham [6]	22.1	−0.51	2809	
Johannsen–Mosaad[a] [23]	23.90	19.40	1294	
Modified Berenson [22]	19.00	−8.70	2809	
Cachard[a] [5]	26.70	11.90	1547	
Present model	14.88	5.20	2809	

[a] Unable to calculate all data points.

new model, overpredict the wall temperatures by a significant margin. This suggests that the heat transfer relations used in these prediction methods are no longer applicable and that the film thickness is overpredicted. Therefore, reliable equations for heat transfer rates for flow in very small gaps are required. A thorough literature survey of such relations is recommended.

Acknowledgements—The financial support provided by the Natural Science and Engineering Research Council of Canada and by AECL is gratefully acknowledged.

REFERENCES

1. Bromley, L. A., Heat transfer in stable film boiling. *Chemical Engineering Progress*, 1950, **46**(5) 211–227.
2. Berenson, P. J., Film-boiling heat transfer from a horizontal surface. *Journal of Heat Transfer*, 1961, **83**, 351–358.
3. Dougall, R. S. and Rohsenow, W. M., Film boiling in the inside of vertical tubes with upward flow of the fluid at low qualities. *MIT Report* 9079-26, 1963.
4. Analytis, G. Th. and Yadigaroglu, G., Analytical modeling of inverted annular film boiling. *Nuclear Engineering Design*, 1987, **99**, 201–212.
5. de Cachard, F., Development, implementation and assessment of specific closure laws for inverted-annular film-boiling in a two-fluid model. *Paul Scherrer Institute (PSI) Report* 94-16, 1994.
6. Denham, M. K., Inverted annular film boiling and the Bromley model. *IChE Symposium Series* 86, 1984, pp. 13–23.
7. Hammouda, N., Subcooled film boiling in non-aqueous fluids. Ph.D. thesis, University of Ottawa, Ottawa, Canada, 1995.
8. Fung, K.K., Subcooled and low quality film boiling of water in vertical flow at atmospheric pressure. Ph.D. thesis, University of Ottawa, Ottawa, Canada, 1981.
9. Stewart, J. C., Low quality film boiling at intermediate and elevated pressures. M.Sc. thesis, University of Ottawa, Ottawa, Canada, 1981.
10. Laperrière, A., An analytical and experimental investigation of forced convective film boiling. M.Sc. thesis, University of Ottawa, Ottawa, Canada, 1983.
11. Hsu, Y. Y. and Westwater, W., Approximate theory for film boiling on vertical surfaces. *Chemical Engineering Progress, AIChE, Heat Transfer Conference*, Storrs, CT, 1959, Vol. 56, pp. 15–24.
12. Ishii, M., *Thermo-fluid Dynamic Theory of Two-Phase Flow*. Eyrolles, 1975.
13. Delhaye, J. M., Equations fondamentales des écoulements diphasiques. CEA-R-3429, 1969.
14. Delhaye, J. M., Basic equations for two-phase flow modeling. In *Two-Phase flow and Heat Transfer in the power and process industries*, ed. A. E. Bergles, J. G. Collier, J. M. Delhaye, G. F. Hewitt and F. Mayinger, Hemisphere Publishing, New York, 1981.
15. Ishii, M. and Mishima, K., Two-fluid and hydrodynamic constitutive relations. *Nuclear Engineering and Design*, 1984, **86**.
16. Yardigaroglu, G. and Lahey, R. T., On the various forms of the conservation equations in two-phase flow. *International Journal of Multiphase Flow*, 1975, **2**, 477–494.
17. Dittus, F. W. and Boelter, L. M. K., *Heat Transfer in Automobile Radiators of the Tubular Type*. University of California Publications, 1930, Vol. 2, 443–461.

18. Kays, W. M. and Crawford, M. E., *Convective Heat and Mass Transfer*, 2nd edn. McGraw-Hill, New York, 1980.
19. Bhatti, M. S. and Shah, R. K., Turbulent and transition flow convective heat transfer in ducts. In *Handbook of Single-Phase Convective Heat Transfer*, ed. S. Kalkaç, R. K. Shah and W. Aung. John Wiley, New York, 1987.
20. Siegel, R. and Howell, J. R., *Thermal Radiation Heat Transfer*. McGraw-Hill, New York, 1972.
21. Hammouda, N., An experimental study of subcooled film boiling of refrigerants in vertical up-flow. *International Journal of Heat and Mass Transfer*, 1996, **39**, 3799–3812.
22. Leung, L. K. H. and Groeneveld, D. C., Development of post-dryout look-up table for loss-of-regulation accident conditions. Atomic Energy of Canada, unpublished report, 1988.
23. Johannsen, K. and Mosaad, M., A new correlation for subcooled and low quality film boiling heat transfer of water at pressures from 0.1 to 8 MPa. *Proceedings of the 4th International Topical Meeting on Nuclear Reactor Thermal-Hydraulics*, 1989, Vol. 2, pp. 10–13.
24. Hammouda, N., A review and assessment of prediction methods for post-dryout heat transfer. Atomic Energy of Canada, unpublished report, 1995.